Observation of the splitting of degenerate surface plasmon polariton modes in a two-dimensional metallic nanohole array

Lin Pang,[a] Kevin A. Tetz, and Yeshaiahu Fainman
Department of Electrical and Computer Engineering, University of California, San Diego, 9500 Gilman Drive, La Jolla, California 92093-0407

(Received 8 December 2006; accepted 5 February 2007; published online 12 March 2007)

The authors report the experimental observation of the splitting of the degenerate $(0,\pm1)$ surface plasmon polariton modes excited in a metallic nanohole array integrated with microfluidic channel for delivery and precise control of the index of refraction of overlaying layer. They use high-resolution wavelength and angle scans for excitation of the surface modes and a polarizer-analyzer pair to suppress the nonresonant transmission. The two resultant modes include an intense, spectrally broad low-energy mode and a weaker, much narrower bandwidth high-energy mode. © *2007 American Institute of Physics*. [DOI: 10.1063/1.2713145]

The unique properties of surface plasmon polaritons (SPPs) (i.e., surface confinement, maximum amplitude value on the surface of the interface, and longitudinal nature) have attracted various attentions including nanophotonics, optoelectronics, and biophotonics.[1,2] Recent awareness of SPP modes has been sparked after reports of enhanced transmission through optically thick metal film with subwavelength features.[3,4] The interaction between these modes will open an energy band gap or reduce the radiative damping of the SPP fields.[5–7] Both simulation studies and measurements indicate the formation of low-energy and high-energy modes with symmetric and antisymmetric electric field distributions, respectively.[4,7–11] Band gaps in the SPP dispersion could also be generated from the SPP Bragg scattering.[12–15] It is evident that experiments on the study of interaction between the SPP modes have had partial success due to the presence of a strong nonresonant background term.[11,16,17] In this letter, we describe techniques to suppress the nonresonant transmission, revealing the mechanism of interaction among SPP modes. We observe a band gap at normal incidence due to the strong interference among four $(\pm1,\pm1)$ SPP modes and the splitting of the two degenerate $(0,\pm1)$ modes.

We employ a polarizer-analyzer (PA) pair to eliminate the nonresonant transmission, use a collimated tunable laser beam with 1 pm wavelength resolution (1520–1570 nm, 6.9 dBm) and a rotation stage of 0.001° angle resolution to excite a SPP field, and utilize a microfluidic channel for delivery and precise control of the index of refraction of overlaying layer on top of the metallic two-dimensional (2D) hole array. The sample [see Refs. 18 and 19 for the fabrication of gold hole array and the assembly of a microfluidic channel $(20\times2\times0.1\ \mathrm{mm}^3)$] is inserted between a PA pair and excited with collimated beam [see Fig. 1(a)]. The transmitted light is used to simultaneously image an area of $\sim200\times200\ \mu\mathrm{m}^2$ of the sample onto an InGaAs camera for alignment as well as a photodiode for transmission measurements.[18] The continuous change of the in-plane wave vector was achieved by rotating the sample in the *x*-*z* plane (angle θ).

A 20% Na_2CrO_4 water solution in weight was introduced into the microfluidic channel on an array with a period of 1.65 μm. First, the polarizer and analyzer were paralleled and oriented at 0° (the [1, 0] direction), yielding components of the incident electric field in the $[\pm1,\pm1]$ directions to effectively excite the liquid-metal (LM) $(\pm1,\pm1)$ modes. In Fig. 1(b), the transmission spectra clearly shows LM $(\pm1,\pm1)$, LM (1, 0), and substrate-metal (SM) $(\pm1,\pm1)$, $(-2,0)$ modes. The dispersion curves in Fig. 1(b) were calculated using standard SPP dispersion equations[20] with effective dielectric constants of 2.10, 1.75, and $-95+11i$ for glass, liquid, and gold, respectively. Figure 1(c) is a zoom-in in the vicinity of normal incidence excitation, distinctly showing an anticrossing of the SPP modes with an energy bang gap of about 2.1 meV (~5 nm) similar to the results reported in Ref. 7. For a better understanding of the effects, we suppressed the directly transmitted nonresonant background by using an orthogonally crossed PA pair, leading to a change of the resonance from broad Fano type to narrower Lorentzian line shape.[18] The latter is accomplished by orienting the po-

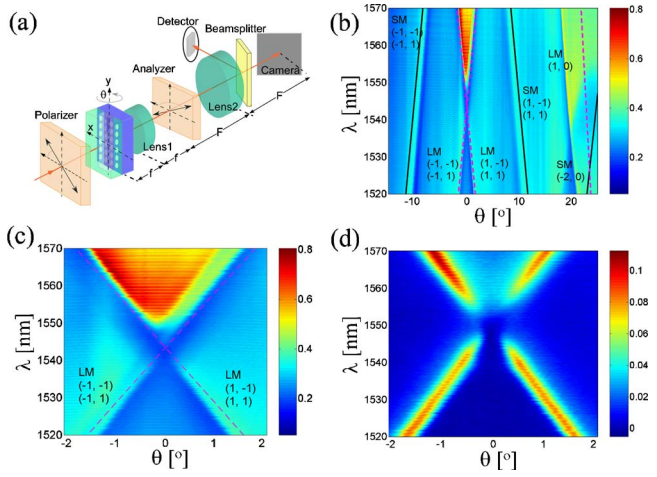

FIG. 1. (Color online) (a) Schematic of the experiment. The polarization states of a laser beam are controlled by a polarizer to provide variable excitation. A microfluidic channel is used to transport the index adjusting fluid to the metal surface to turn the SPP resonance frequency. (b) Angle-resolved transmission for a 2D array with period of 1.65 μm for the parallel PA pair ([1,0] direction) along with calculated SPP modes: black solid for SM and magenta dashed for LM modes. (c) Zoom-in of (b) in the vicinity of normal incidence. (d) Transmission of LM $(\pm1,\pm1)$ with the PA orthogonally oriented.

[a]Electronic mail: lpang@ece.ucsd.edu

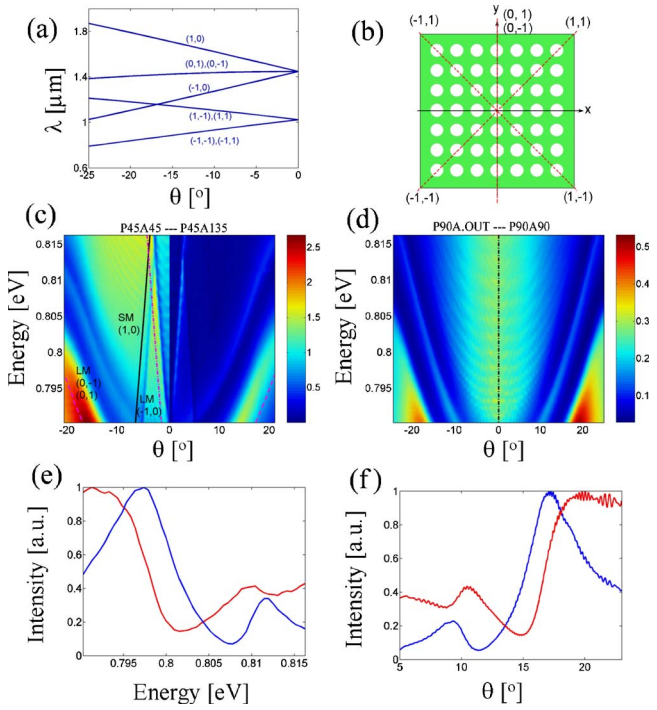

FIG. 2. (Color online) (a) Dispersion curve of LM SPPs. (b) Schematic of the array and propagating directions of the SPP modes. (c) Angle-resolved transmission for a 2D array with 1.0 μm period for the parallel PA pair oriented at 45° (the left side) and orthogonal orientation (the right side, the intensity is five times lower than that of the left side) along with calculated LM $(0,\pm1)$ (magenta dashed), LM $(-1,0)$ (magenta dash dot), and SM (1, 0) (black solid) modes. (d) Transmission for the parallel PA pair oriented at 90° to [1, 0] direction (the right side) and polarizer at 90° without analyzer (the left side). (e) Normalized spectral transmission at 18° incidence excitation for orthogonal (blue) and parallel (red) PA orientations. (f) Normalized angular transmission at 1560 nm for orthogonal (blue) and parallel (red) PA orientations to show the splitting of the degeneration.

larizer at 22.5° and the analyzer at 112.5° with respect to the [1, 0] direction. In the vicinity of normal incidence, there are well-defined variations of linewidth and the transmitted intensities. More importantly, pronounced near-zero intensity can be clearly observed within the band gap [see Fig. 1(d)]. In comparison to the parallel PA pair [Fig. 1(c)], the transmission peak in Fig 1(d) is redshifted with the crossing point shifting from 1534 to 1550 nm. Changing from Fano type to Lorentzian resonance shape (i.e., replacing parallel PA pair by orthogonal one), we achieved an enhanced observation of the interaction between SPP modes without losing any important band structure information except an expected slight shift of the center of the energy band gap position.

Among the four $(\pm1,\pm1)$ modes, $(1,-1)$ and (1, 1) are degenerate, and so are $(-1,-1)$ and $(-1,1)$ modes [see Figs. 1(c) and 2(a)]. After being excited, the degenerate modes $(1,-1)$ and (1, 1) will propagate orthogonally along the [1, −1] and [1, 1]directions, respectively [see Fig. 2(b)]. Since the SPP waves are longitudinal, the electric fields of these two modes are also orthogonally polarized; they will not interact. As a result, they will stay degenerate. This also applies to the $(-1,-1)$ and $(-1,1)$ modes. However, at normal excitation, the $(1,-1)$ and $(-1,1)$ modes will interfere due to their collinear electric fields; the same situation holds for (1, 1) and $(-1,-1)$ modes [see Fig. 2(b)]. The anticrossing of these four modes leads to the formation of the energy band gap.

Figure 2(a) shows another pair of degenerate $(0,\pm1)$ modes. At normal incidence, these two degenerate modes cross over with the two nondegenerate $(\pm1,0)$ modes. In contrast to the $(1,\pm1)$ or $(-1,\pm1)$ modes, the degenerate $(0,\pm1)$ modes have collinear propagation directions at any excitation angle, which means that these two modes will interact at any in-plane wave vector in the SPP dispersion relation. The interference between these two modes would result in the splitting of the degenerate $(0,\pm1)$ modes. In order to confirm the prediction, we conducted experiments with an array of 1.0 μm period and used index matching fluid to tune the SPP modes. For efficient excitation of the LM $(\pm1,0)$ and LM $(0,\pm1)$ SPP modes, we set the polarization state of the incident optical field at 45° to the [1, 0] direction. Figure 2(c) shows the transmission spectra for parallel PA pair oriented at 45° (the left side) and orthogonal orientation with polarizer oriented at 45° and analyzer at 135° to the [1, 0] direction (the right side). LM $(\pm1,0)$, LM $(0,\pm1)$, and SM $(\pm1,0)$ modes were clearly resolved. The liquid (oil) dielectric constant of 2.57 was used to fit in the calculated dispersion curve [see Fig. 2(c)]. As expected, the interference between the LM (0, 1) and LM $(0,-1)$ modes leads to the formation of two separate SPP eigenmodes of different spatial symmetries clearly resolved in both PA orientations. The resultant modes observed in Fig. 2(c) consist of a broad and intense resonance at lower energy with a full width at half maximum (FWHM) of about ~10 meV (~17 nm) and a much narrower resonance at higher energy with a FWHM of about ~5 meV (~8 nm). The energy separation between these two resonances is ~14.5 meV (27 nm) [see, Fig. 2(e)]. The angular bandwidths for the high- and low-energy modes are 2.1° and 5°, respectively [Fig. 2(f)]. To observe the nature of the $(0,\pm1)$ mode splitting, we set the polarizer to [0, 1] orientation (y axis) to excite only LM $(0,\pm1)$ modes and set the analyzer to the same orientation or just take it out. The slight change of oil concentration causes a slight shift of the resonant frequency [Fig. 2(d)]. The right part in Fig. 2(d) corresponds to the parallel PA pair along the [0, 1] direction, whereas the left counterpart corresponds to the case when the analyzer is absent. As we anticipated, only LM $(0,\pm1)$ modes were excited; the splitting of the $(0,\pm1)$ modes could clearly be observed in both cases with almost the same distribution except for a slight intensity difference.

Figure 2(a) shows that the $(\pm1,0)$ and $(0,\pm1)$ modes will coincide at normal excitation. With the splitting of the two $(0,\pm1)$ modes, a crossing shift should be expected. To observe this phenomenon, we tuned the resonant excitations by changing the dielectric constant of the fluid to 2.381. Figure 3(a) shows the transmission for a parallel PA pair oriented at 45°. We can clearly observe that the LM $(0,\pm1)$ modes no longer coincide at the crossing point of the nondegenerate LM $(\pm1,0)$ modes. A diamondlike shape around the intersection at about 1530 nm is revealed [arrow in Fig. 3(a)], resulting from the splitting of two generate LM $(0,\pm1)$ modes. For further clarification in the vicinity of normal incidence, we changed PA into the orthogonal orientation [see Fig. 3(b)] with slightly condensed oil to shift the SPP modes to longer wavelength. We can distinguish the intense, low-energy and the weaker, high-energy modes in the spectra. These two modes lay outside the crossing areas of the two nondegenerate LM $(\pm1,0)$ modes. Interactions between the LM $(\pm1,0)$ modes and the split modes lead to the diamond-

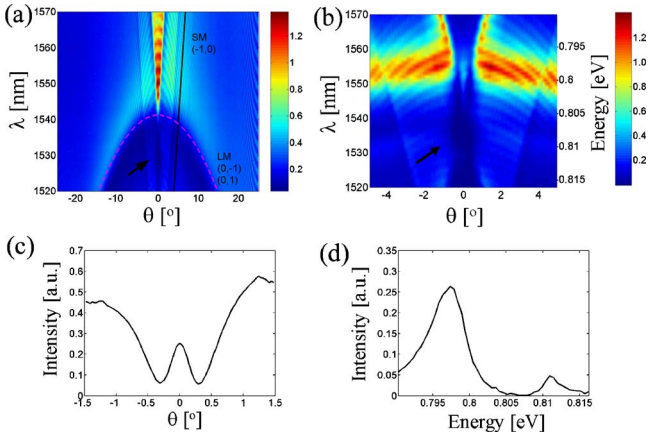

FIG. 3. (Color online) (a) Angle-resolved transmission for the array with 1.0 μm period for the parallel PA pair oriented at 45° along with calculated LM $(0,\pm1)$ (magenta dashed) and SM $(-1,0)$ (black solid) modes [for clarity, LM $(\pm1,0)$ and SM (1, 0) are not shown]. (b) Transmission for the orthogonal PA pair oriented at 45° and analyzer at 135° in the vicinity of normal excitation. (c) Angular transmission at 1549 nm of (b) from −1.5° to 1.5° showing the low-energy mode "trapped" between the LM $(\pm1,0)$ modes.(d) Spectral transmission at 0.3° incidence to show the energy bandwidth of these two modes.

like shape of the intersection [arrow in Fig. 3(b)] and the formation of "isolated" spots at certain locations [especially the bright spot between the LM $(\pm1,0)$ modes in Fig. 3(b) around 0.8 eV]. The angular linewidth of this spot is 0.3° [see Fig. 3(c)], smaller than the linewidth of the LM $(\pm1,0)$ and SM $(\pm1,0)$, which are 0.5° and 0.8° (not shown), respectively. Figure 3(d) shows a spectrum near normal incidence (−0.3°); even the spot for the high-energy mode (at 0.811 eV) can be seen. The linewidth of spots for the high- and low-energy modes are 3 (~5 nm) and 6 meV (~11 nm), respectively. The separation between these two modes is ~14 meV (26 nm), consistent with the measurement far away from the normal incidence [see Fig. 2(e)].

The origin of the splitting of the degenerate modes can be understood from the microscopic pictures of the electric field and the corresponding intensity distribution at the metal surface. Two solutions may be expressed as two standing waves resulting from the coupling of the excited uncoupled $(0,\pm1)$ modes: the symmetric $S\sim[\exp(ik_{sp}y)+\exp(-ik_{sp}y)]\sim\cos(k_{sp}y)$ and the antisymmetric $A\sim[\exp(ik_{sp}y)-\exp(-ik_{sp}y)]\sim\sin(k_{sp}y)$. The intensity distributions for these two modes are such that the maxima and minima coincide with the hole locations for the S and A modes, respectively.[7] Moreover, the symmetric S and antisymmetric A modes occur at different photon energies [see Fig. 3(d)]; the higher energy for A mode is due to the surface charges and the distortion of its electric field.[13] The total strength of the scattered field by the nanoholes is higher for symmetric S mode due to higher radiative damping.[7]

In conclusion, we have investigated the mode interference among the SPP modes in a 2D metallic nanohole array integrated with microfluidic channel for the delivery and precise control of the index of refraction of overlaying layer using spectroscopy with a PA pair, high-resolution wavelength, and angle scans. We observed the strong coupling among SPP modes at the normal excitation, and more importantly, the splitting of the two degenerate $(0,\pm1)$ modes, leading to the formation of the symmetric and antisymmetric modes with an energy separation of ~14 meV. The collinear propagating directions of uncoupled SPP $(0,\pm1)$ modes contribute to the pronounced splitting in the dispersion relation.

This work was partially funded by the DARPA Center for Opto-Fluidic Integration, NSF, and AFOSR.

[1]H. Raether, *Surface Plasmons on Smooth and Rough Surfaces and on Gratings* (Springer, Berlin, 1988).
[2]W. L. Barnes, A. Dereux, and T. W. Ebbesen, Nature (London) **424**, 824 (2003).
[3]T. W. Ebbesen, H. J. Lezec, H. F. Ghaemi, T. Thio, and P. A. Wolff, Nature (London) **391**, 667 (1998).
[4]L. Martin-Moreno, F. J. Garcia-Vidal, H. J. Lezec, K. M. Pellerin, T. Thio, J. B. Pendry, and T. W. Ebbesen, Phys. Rev. Lett. **86**, 1114 (2001).
[5]S. C. Hohng, Y. C. Yoon, D. S. Kim, V. Malyarchuk, R. Muller, Ch. Lienau, J. W. Park, K. H. Yoo, J. Kim, H. Y. Ryu, and Q. H. Park, Appl. Phys. Lett. **81**, 3239 (2002).
[6]P. Paddon and J. F. Young, Phys. Rev. B **61**, 2090 (2000).
[7]C. Ropers, D. J. Park, G. Stibenz, G. Steinmeyer, J. Kim, D. S. Kim, and C. Lienau, Phys. Rev. Lett. **94**, 113901 (2005).
[8]D. Gerard, L. Salomon, F. de Fornel, and A. V. Zayats, Opt. Express **12**, 3652 (2004).
[9]S. A. Darmanyan, M. Neviere, and A. V. Zayats, Phys. Rev. B **70**, 075103 (2004).
[10]A. Krishnan, T. Thio, T. J. Kim, H. J. Lezec, T. W. Ebbesen, P. A. Wolff, J. Pendry, L. Martin-Moreno, and F. J. Garcia-Vidal, Opt. Commun. **200**, 1 (2001).
[11]A. Degiron, H. J. Lezec, W. L. Barnes, and T. W. Ebbesen, Appl. Phys. Lett. **81**, 4327 (2002).
[12]S. C. Kitsin, W. L. Barnes, and J. R. Sambles, Phys. Rev. B **52**, 11441 (1995).
[13]W. L. Barnes, T. W. Preist, S. C. Kitsonand, and J. R. Sambles, Phys. Rev. B **54**, 6227 (1996).
[14]S. C. Kitson, W. L. Barnes, G. W. Bradberry, and J. R. Sambles, J. Appl. Phys. **79**, 8373 (1996).
[15]M.-W. Tsai, T.-H. Chuang, H.-Y. Chang, and S.-C. Lee, Appl. Phys. Lett. **88**, 213112 (2006).
[16]M. Sarrazin, J. P. Vigneron, and J. M. Vigoureux, Phys. Rev. B **67**, 085415 (2003).
[17]C. Genet, M. P. van Exter, and J. P. Woerdman, Opt. Commun. **225**, 331 (2003).
[18]K. Tetz, L. Pang, and Y. Fainman, Opt. Lett. **31**, 1528 (2006).
[19]L. Pang, W. Nakagawa, and Y. Fainman, Appl. Opt. **42**, 5450 (2003).
[20]K. A. Tetz, R. Rokitski, M. Nezhad, and Y. Fainman, Appl. Phys. Lett. **86**, 111110 (2005).